

Theoretical Investigation of the $\text{CO}_2 + \text{OH}^- \rightarrow \text{HCO}_3^-$ Reaction in the Gas and Aqueous Phases

Z. Peng[†] and Kenneth M. Merz, Jr.*

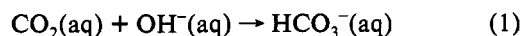
Contribution from the Department of Chemistry, 152 Davey Laboratory, The Pennsylvania State University, University Park, Pennsylvania 16802

Received March 15, 1993*

Abstract: For the $\text{CO}_2 + \text{OH}^- \rightarrow \text{HCO}_3^-$ reaction in the gas phase, we have identified the minimum energy reaction path using high-level *ab initio* calculations. The gas-phase free energy profile at 298.15 K has been assembled by computing thermodynamic corrections, which are quite significant. The full thermodynamic cycles for this reaction in the gas and aqueous phases have been constructed. The main feature of the gas-phase results is that the reaction is activationless, which agrees with previous theoretical studies. We have also performed molecular dynamics free energy perturbation simulations on this system in an aqueous environment. Our results predict an aqueous free energy barrier (19.2 kcal/mol) which is induced by solvation effects. The ramifications of our results on the catalytic mechanism of carbonic anhydrase are discussed.

1. Introduction

The reaction of CO_2 with OH^- has an important biological role in blood pH regulation and the transportation of CO_2 in living systems.¹ Experiments show that the forward reaction (eq 1) in an aqueous environment encounters an activation energy



(E_a) barrier of 13.25 kcal/mol,² which is too high to be physiologically useful.¹ However, nature provides an enzyme, carbonic anhydrase (CA), to speed up the reaction by 7 orders of magnitude, which makes this enzyme reaction one of the fastest known.³ Thus, the origin of the aqueous-phase activation barrier is one of the key issues in furthering our understanding of the catalytic action of CA.³

Previous theoretical studies of this reaction in the gas phase by Jönsson *et al.*⁴ and by Liang and Lipscomb⁵ showed that there is no activation barrier on the gas phase energy profile. This led to the speculation^{4,5} that the solution-phase barrier is induced solely by solvation effects. A study based on a continuum solvation model by Miertus *et al.* did show qualitatively a solvation-induced activation barrier.⁶

However, the origin of the activation barrier still remains an open issue for three reasons. First, the basis sets used in the previous gas-phase *ab initio* studies^{4,5} are relatively small by today's standard, especially when dealing with a charged system. The calculated ΔE_{rxn} varies significantly with the basis sets used and the treatment of electron correlation: −56 kcal/mol

(double- ζ quality basis set augmented by diffuse s and p functions on carbon and oxygen),⁴ −82.6 kcal/mol (4-31G),⁵ −60.3 kcal/mol (4-31+G),⁵ and finally −40.0 kcal/mol (MP2//4-31+G).⁵ Clearly, the ΔE_{rxn} is far from being converged. For comparison, the experimentally estimated heat of reaction (ΔH_{rxn}) in the gas phase is −49 kcal/mol.⁵ Secondly, the effect of finite temperature was not included.^{4–6} At finite temperature, the thermodynamic quantity which determines the direction and rate of a chemical reaction is free energy, and the enthalpy, entropy, and free energy contributions from the molecular translational, vibrational, and rotational motions could be very important.^{7,8} Thirdly, explicit solvent effects have not been considered at the molecular level⁶ (recently Aqvist *et al.* have reported a molecular-level study of this reaction (see ref 31)).

In a recent letter,⁹ we used extended basis sets (up to the 6-311++G** level) with electron correlation included up to the MP4 level, finite temperature corrections to obtain thermodynamic quantities, and molecular dynamics¹⁰ free energy perturbation¹¹ (MD-FEP) runs for explicit solvation treatment to demonstrate how important the aforementioned points are with regard to this reaction. In this paper, we present a more detailed account of our work. In section 2, the general methodology employed in this study will be presented. In section 3, we will discuss the results from the *ab initio* calculations and use them to construct the relevant thermodynamic cycles and reaction profiles for this reaction in the gas phase. Next the results from the MD-FEP simulations in the aqueous phase will be presented. The aqueous-phase free energy profile obtained in this way will then be compared with experimental observations. The paper is

[†] Current address: Biosym Technologies, Inc., 9685 Scranton Road, San Diego, CA 92121.

* Abstract published in *Advance ACS Abstracts*, September 15, 1993.

(1) (a) Maren, T. H. *Physiol. Rev.* **1967**, *47*, 595. (b) Davis, R. E. *Biol. Rev. Cambridge Philos. Soc.* **1951**, *26*, 87. (c) Roughton, F. J. W. *Harvey Lect.* **1943**, *39*, 96. (d) Kerm, D. M. *J. Chem. Educ.* **1960**, *14*, 37.

(2) Pinsent, B. R. W.; Pearson, L.; Roughton, F. J. W. *Trans. Faraday Soc.* **1956**, *52*, 1512.

(3) For recent reviews, see: (a) Silverman, D. N.; Lindskog, S. *Acc. Chem. Res.* **1988**, *21*, 30. (b) Silverman, D. N.; Vincent, S. H. *CRC Crit. Rev. Biochem.* **1983**, *14*, 207. (c) Lipscomb, W. N. *Annu. Rev. Biochem.* **1983**, *52*, 17. (d) Lindskog, S. In *Zinc Enzymes*; Spiro, T. G., Ed.; John Wiley & Sons: New York, 1983. (e) Pocker, Y.; Sarkanen, S. *Adv. Enzymol. Relat. Areas Mol. Biol.* **1978**, *47*, 149. (f) Bertini, I.; Luchinat, C.; Scozzafava, A. *Struct. Bonding (Berlin)* **1981**, *48*, 45. See also ref 24.

(4) Jönsson, B.; Karlstrom, G.; Wennerstrom, H. *J. Am. Chem. Soc.* **1978**, *100*, 1658.

(5) Liang, J. Y.; Lipscomb, W. N. *J. Am. Chem. Soc.* **1986**, *108*, 5051.

(6) Miertus, S.; Kysel, O.; Krajcik, K. *Chem. Zvesti* **1981**, *35*, 3.

(7) Del Bene, J. E.; Mettee, H. D.; Frisch, M. J.; Luke, B. T.; Pople, J. A. *J. Phys. Chem.* **1983**, *87*, 3279.

(8) Hehre, W. J.; Radom, L.; Schleyer, P. v. R.; Pople, J. A. *Ab initio Molecular Orbital Theory*; John Wiley & Sons, Inc.: New York, 1986 and the relevant references therein.

(9) Peng, Z.; Merz, K. M., Jr. *J. Am. Chem. Soc.* **1992**, *114*, 2733.

(10) For general references on MD techniques, see: (a) Brooks, C. L.; III; Karplus, M.; Pettit, B. M. *Proteins: A Theoretical Perspective of Dynamics, Structures, and Thermodynamics*; Advances in Chemical Physics, Vol. 71; John Wiley & Sons: New York, 1988. (b) McCammon, J. A.; Harvey, S. C. *Dynamics of Proteins and Nucleic Acids*; Cambridge University Press: London, 1987. (c) Allen, M. P.; Tildesley, D. J. *Computer Simulation of Liquids*; Clarendon Press: Oxford, U.K., 1987. (d) van Gunsteren, W. F.; Berendsen, H. J. C. *Angew. Chem., Int. Ed. Engl.* **1990**, *29*, 1023 and references therein.

(11) For general references on FEP, see: (a) Mezei, M.; Beveridge, D. L. *Ann. N. Y. Acad. Sci.* **1986**, *482*, 1. (b) van Gunsteren, W. F. *Protein Eng.* **1988**, *2*, 5. (c) Jorgensen, W. L. *Acc. Chem. Res.* **1989**, *22*, 184. (d) Beveridge, D. L.; DiCapua, F. M. *Annu. Rev. Biophys. Biophys. Chem.* **1989**, *18*, 431. (e) Kollman, P. A.; Merz, K. M., Jr. *Acc. Chem. Res.* **1990**, *23*, 246.

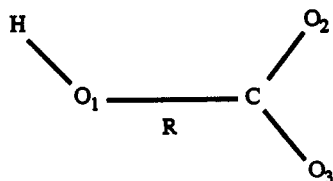


Figure 1. Labeling of the $\text{OH}^-\cdots\text{CO}_2$ complex. The distance R between O_1 and C is the reaction coordinate.

concluded with a discussion on the ramifications of our observations on the catalytic mechanism of CA.

2. Methods

The *ab initio* gas-phase reaction profile was studied using Gaussian 88.⁸ The reaction coordinate R was chosen to be the distance between the O_1 atom of the hydroxide ion and the C atom of carbon dioxide (see Figure 1), which has also been used in previous studies.^{4,5} Our choice of using a simple reaction coordinate model instead of more sophisticated intrinsic minimum energy reaction coordinate methods¹² was mainly based on simplicity. However, it has been shown that useful chemical insights can be obtained using methods that generate reaction profiles other than the intrinsic minimum energy reaction coordinate.¹³

Initially, we carried out full RHF optimizations at the 6-31+G** level to identify the minimum energy conformations of HCO_3^- , OH^- , and CO_2 . Next we carried out full geometry optimizations where we fixed the value of R at values between ~ 1.4 and ~ 10.0 Å. The molecular electric dipole moment⁸ and the ESP-derived atomic point charges¹⁴ at each molecular conformation along the reaction profile were also obtained from the same calculations using Gaussian 88.⁸

Since we do not have a real energy minimum for any molecular conformation along the reaction profile (other than the fully minimized HCO_3^- , OH^- , and CO_2), we could not use conventional methods to calculate the thermodynamic contributions from the molecular vibration, rotation, and translation motions.^{7,8} We bypassed this difficulty by removing the contribution of the reaction coordinate R from the energy gradient vector \mathbf{G} and Hessian matrix \mathbf{H} .¹⁵ This was done in the following way. At each molecular conformation along the reaction profile, a projection operator \mathbf{P} was constructed

$$\mathbf{P} = \mathbf{I} - \mathbf{n}\mathbf{n}^+ \quad (2)$$

where \mathbf{I} is the $3N \times 3N$ identity matrix (N is the number of atoms in the system under consideration) and \mathbf{n} is a unit vector along the energy gradient vector \mathbf{G} (this is along the reaction coordinate R). We then let \mathbf{P} operate on the energy gradient \mathbf{G} and Hessian matrix \mathbf{H}

$$\mathbf{G}' = \mathbf{P}\mathbf{G} \Rightarrow 0 \quad (3.1)$$

$$\mathbf{H}' = \mathbf{P}\mathbf{H}\mathbf{P} \quad (3.2)$$

\mathbf{G}' and \mathbf{H}' are the energy gradient vector and Hessian matrix without the contribution from the reaction coordinate R . Because the reaction profile was constructed in such a way that the energy was a minimum in the subspace (less the reaction coordinate R) of the molecular conformation space, it is easy to see that \mathbf{G}' has to be zero and \mathbf{H}' supports $3N - 7$ modes of molecular vibration. The new Hessian matrix \mathbf{H}' was then used to calculate the molecular vibrational frequencies. Since the HF-calculated vibration frequencies have been shown to be systematically larger than the experimentally observed ones,⁸ a scaling factor of 0.9 was used to scale down the RHF/6-31+G** calculated vibration frequencies. Finally the thermodynamic contributions of the molecular vibration ($3N - 7$

modes), rotation, and translation (at 298.15 K) were calculated using conventional methods.^{7,8}

There are still two more difficulties left to be taken into consideration. First, there will be only $3N - 7$ vibration modes for most molecular conformations along the reaction profile except for the fully optimized HCO_3^- , which has $3N - 6$ modes of vibration, and the isolated OH^- and CO_2 , which together have $3N - 12$ modes of vibration since six modes of intermolecular vibrations transform into three rigid translational and three rotational motions. As we shall see later, this results in discontinuities in the reaction profile. The second difficulty is related to the harmonic oscillator approximation used in the enthalpy and entropy calculations.^{7,8} When the distance between OH^- and CO_2 increases, the frequencies of the intermolecular vibration modes can drop below kT (about 200 cm^{-1} at room temperature) and the harmonic oscillator approximation is no longer valid, especially in the entropy calculation.^{7,8} This will be touched on in more detail later.

In order to assess the importance of electron correlation, MP2/6-31+G**//RHF/6-31+G** calculations⁸ at several points along the reaction profile were also conducted. Full MP2/6-31+G** optimizations on HCO_3^- , CO_2 and OH^- were also performed. The results of this study suggested the necessity of using larger basis sets and better electron correlation treatments. We then redid the optimizations at several (not all because of the size of the calculation) R points along the reaction profile at the RHF/6-311++G** level. The RHF/6-311++G** molecular geometries changed only slightly with respect to the RHF/6-31+G** values. Finally, the energetics of these points were evaluated at the MP4/6-311++G**//RHF/6-311++G** level and the full energy profile was then interpolated from these points. No correction for BSSE¹⁶ was considered due to the size of the computation and also the controversy surrounding the merit of such a correction.¹⁷ After all the calculations in the gas phase were completed, the reaction profiles of energy (E_{gas}), enthalpy (H_{gas}), entropy (S_{gas}), and free energy (G_{gas}) were constructed.

Molecular dynamics free energy perturbation (MD-FEP)^{10,11} simulations were performed in order to obtain the free energy of solvation (ΔG_{sol}) along the reaction profile obtained from the *ab initio* gas-phase calculations. This will take into account the effect of solvation, and the free energy profile G_{aq} for the reaction in an aqueous environment will be approximated by the sum of the gas-phase free energy profile G_{gas} and ΔG_{sol} . AMBER 3.0A was used.¹⁸ Bond, angle, and torsion parameters were chosen to make the $\text{OH}^-\cdots\text{CO}_2$ complexes rigid in order to keep the molecular geometries near their gas-phase *ab initio* calculated values. The solvent molecules (water) interact with the $\text{OH}^-\cdots\text{CO}_2$ solute complexes via the nonbond electrostatic and van der Waals terms, and the TIP3P water model was used.¹⁹ The atomic point charges of the solute complexes came directly from the *ab initio* gas-phase ESP-fitting procedure at the RHF/6-31+G** level.¹⁴ The van der Waals parameters for the two end points on the reaction profile were parameterized such that the experimental free energies of solvation of HCO_3^- , OH^- , and CO_2 were closely reproduced.²⁰ Then the van der Waals parameters for other points along the reaction profile were interpolated from the corresponding end point values, assuming that the functional behavior of the van der Waals parameters along the reaction profile is similar to that of the RHF/6-31+G** energy profile. This appears to be a good assumption, especially when the functional behaviors of the ESP-derived atomic point charges are considered. This point will be discussed further below. The nonbond cutoff distance was 8.0 Å,^{10,11} SHAKE was used to constrain all bond lengths,²¹ the time-step was 1.5 fs,^{10,11} and periodic boundary conditions were employed in all simulations.^{10,11} The temperature and pressure were maintained at 298.15 K and 1.0 atm, respectively.^{10,11} A typical MD-FEP run involved energy minimization of the system (a box of ~ 500 or more TIP3P¹⁹ water molecules solvating a $\text{OH}^-\cdots\text{CO}_2$ complex), followed by 45 ps of MD equilibration. Electrostatic decoupling

(16) Boys, S. F.; Bernardi, F. *Mol. Phys.* 1970, 19, 553.

(17) (a) Schwenke, D. W.; Truhlar, D. G. *J. Chem. Phys.* 1985, 82, 2418.

(b) Frisch, M. J.; Del Bene, J. E.; Binkley, J. S.; Schaefer, H. F., III. *J. Chem. Phys.* 1986, 84, 2279. (c) Dannenberg, J. J.; Mezei, M. *J. Phys. Chem.* 1991, 95, 6396.

(18) Seibel, G.; Singh, U. C.; Weiner, P. K.; Caldwell, J.; Rollman, P. A. AMBER 3.0A.

(19) Jorgensen, W. L.; Chandrasekhar, J.; Madura, J. D.; Impey, R. W.; Klein, M. L. *J. Chem. Phys.* 1983, 79, 926.

(20) (a) Wilhelm, E.; Battino, R.; Wilcock, R. *J. Chem. Rev.* 1977, 77, 231. (b) Ben-Naim, A.; Marcus, Y. *J. Chem. Phys.* 1984, 81, 2016. (c) Marcus, Y. *Ion Solvation*; John Wiley & Sons Ltd.: New York, 1985; pp 107. (d) Marcus, Y.; Loewenschuss, A. *Annu. Rep. Prog. Chem., Sect. C* 1984-1985, 81-135. (e) Marcus, Y. *J. Chem. Soc., Faraday Trans. 1* 1987, 83, 339.

(21) van Gunsteren, W. F.; Berenssen, H. J. C. *Mol. Phys.* 1977, 34, 1311.

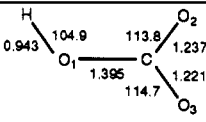
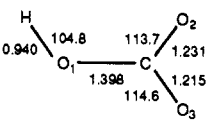
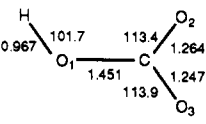
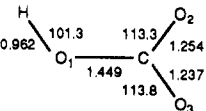
(12) (a) Fukui, K. *J. Phys. Chem.* 1970, 74, 4161. (b) Fukui, K.; Kato, S.; Fujimoto, H. *J. Am. Chem. Soc.* 1975, 97, 1. (c) Kato, S.; Kato, H.; Fukui, K. *J. Am. Chem. Soc.* 1977, 99, 684. (d) Schaefer, H. F., III. *Chem. Br.* 1975, 11, 227. (e) Ishita, K.; Morokuma, K.; Komonicki, A. *J. Chem. Phys.* 1977, 66, 2153. (f) Miller, W. H.; Handy, N. C.; Adams, J. E. *J. Chem. Phys.* 1980, 72, 99. For a more recent review, see: (g) Miller, W. H. In *Perspectives in Quantum Chemistry*; Jortner, J., Pullman, B., Eds.; Kluwer Academic Publishers: Dordrecht, The Netherlands, 1989; pp 57-82 and references therein.

(13) Shida, N.; Almlöf, J.; Barbara, P. F. *J. Phys. Chem.* 1991, 95, 10457.

(14) (a) Williams, D. E.; Yan, J. M.; *Adv. At. Mol. Phys.* 1988, 23, 87. (b) Chirlian, L. E.; Francl, M. M. *J. Comput. Chem.* 1987, 8, 894. (c) Singh, U. C.; Kollman, P. A. *J. Comput. Chem.* 1984, 5, 129.

(15) Peng, Z.; Merz, K. M., Jr. Modifications of Gaussian 88, unpublished work.

Table I. Optimized Geometries^a for OH⁻, CO₂, and HCO₃⁻

basis set	OH ⁻ ^b	CO ₂ ^c	HCO ₃ ⁻ ^d
RHF/6-31+G**	0.947 H—O	1.143 O=C=O	
RHF/6-311++G**	0.945 H—O	1.138 O=C=O	
MP2/6-31+G**	0.969 H—O	1.180 O=C=O	
MP2/6-311++G**	0.965 H—O	1.169 O=C=O	

^a Bonds are in Å and angles are in deg. ^b The experimental H—O bond distance is 0.964 Å (see ref 25). ^c The experimental O—C bond distance is 1.160 Å (see ref 26). ^d All optimized HCO₃⁻ structures are planar

was used in conjunction with a 180-ps slow-growth MD-FEP simulation where the OH⁻...CO₂ complex was slowly annihilated.^{10,11} The first 90 ps evaluated the electrostatic free energy contribution, and the second 90 ps determined the van der Waals free energy contribution. Both forward and backward runs were conducted, and the difference was used as a crude estimation of the error in the MD-FEP simulations.^{10,11} Procedures similar to ours have been utilized by others to study reactions in solution.²²⁻²⁴

3. Results and Discussion

3.1. Gas-Phase Profile. We performed full RHF and MP minimizations on HCO₃⁻, OH⁻, and CO₂ at the 6-31+G** and 6-311++G** levels. The optimized geometries from these calculations are listed in Table I. The RHF-optimized geometries at 6-31+G** and 6-311++G** are very similar; so are the two MP2-optimized structures. Both RHF-optimized structures have shorter bond lengths (by about 0.02 Å) when compared to their MP2-optimized counterparts. It is also interesting to note that the structure optimized at the RHF/6-311++G** level gives the shortest bond lengths while the one optimized at the MP2/6-31+G** level gives the longest. The experimental values for the bond lengths for OH⁻ and CO₂ in the gas phase are 0.964 and 1.160 Å, respectively.^{25,26} Our MP2/6-311++G**-optimized results (0.965 and 1.169 Å) compare quite well with the experimental values. The values obtained by Jönsson *et al.*⁴ are 0.98 and 1.16 Å, respectively. The CO₂ bond length obtained by Liang and Lipscomb⁵ is 1.158 Å, and the O₁-C bond was calculated to be 1.43 Å by Jönsson *et al.*⁴ and 1.426 Å by Liang and Lipscomb.⁵ Our RHF and MP2 results are 1.395, 1.398, 1.451, and 1.449 Å, respectively, thus confirming that the O₁-C bond is indeed relatively long as pointed out by Jönsson *et al.*⁴ In all of our optimized structures of HCO₃⁻, the C—O₂ bond (cis to H—O₁) is longer than the C—O₃ bond (trans to H—O₁) by about 0.01 Å. This was not found either in Jönsson and co-workers

Table II. Gas-Phase Energy Differences between $E(\text{HCO}_3^-)$ and $E(\text{OH}^-) + E(\text{CO}_2)$ (kcal/mol)

geometry optimized at	single-point calculation at the optimized geometries			
	RHF	MP2	MP3	MP4
RHF/DZP ^a	-55.9			
RHF/4-31G ^b	-82.6			
RHF/4-31+G ^b	-60.3	-40.0		
RHF/6-31+G** ^c	-55.1	-48.0	-55.0	-32.3
RHF/6-311++G** ^c	-51.0	-45.0	-49.2	-45.0
MP2/6-31+G** ^c	-55.9	-40.9	-55.3	-47.1
MP2/6-311++G** ^c	-51.1	-44.1	-52.3	-43.7

^a Results from Jönsson *et al.* (see ref 4). ^b Results from Liang and Lipscomb (see ref 5). ^c Current work.

Table III. Calculated Thermodynamic Corrections at 298.15 K^a

	HCO ₃ ⁻	OH ⁻	CO ₂	OH ⁻ + CO ₂	change of reaction
<i>H</i>	18.6	6.7	8.9	15.6	3.0
<i>S</i>	63.5	41.1	50.9	92.0	-28.5
<i>TS</i>					-8.5
<i>G</i> - <i>H</i> - <i>TS</i>					11.5

^a Enthalpy (*H*) and free energy (*G*) are in kcal/mol. Entropy (*S*) is in cal/(mol K), and *TS* is in kcal/mol.

study,⁴ which had the same bond lengths for C—O₂ and C—O₃, or in the Liang and Lipscomb study,⁵ which had the C—O₂ (1.235 Å) bond being shorter than the C—O₃ (1.253 Å) bond. For the latter study this is opposite to what we observe. One of the consistent trends on going from smaller to larger basis sets and on going from RHF to MP2 optimizations is that the H—O₁—C, O₁—C—O₂, and O₁—C—O₃ angles all decrease. For example, the H—O₁—C angle is 106° at RHF/DZP⁴, 104.9° at RHF/6-31+G**, 104.8° at RHF/6-311++G**, 101.7° at MP2/6-31+G**, and 101.3° at the MP2/6-311++G** level (see Table I).

The energies of reaction (ΔE_{reac}) at different levels are given in Table II. One observation from Table II is that the *ab initio* calculations with larger basis sets do improve the estimation of the energy of reaction. However, for this negatively charged system, the energy of reaction does not appear to be well converged even at the 6-311++G** level (see Table II). Moreover, the results from Table II also suggest that electron correlation is quite significant in this system.

The thermodynamic corrections were calculated for the optimized HCO₃⁻, OH⁻, and CO₂ structures at the RHF/6-31+G** level and 298.15 K.^{7,8} The results are summarized in Table III. The total correction to the free energy of reaction is 11.5 kcal/mol, of which 3.0 kcal/mol comes from the enthalpy change and 8.5 kcal/mol is related to the entropy change. Such a large free energy correction confirms that the finite temperature effect is quite important in the study of this reaction. In conjunction with the experimentally determined thermodynamic changes of solvation, we were able to compile the full thermodynamic cycles for this reaction in the gas and aqueous phases (see Figure 2). Our calculated heats of formation in the gas and aqueous phases are estimated to be -42⁴ and -6 kcal/mol,⁵ respectively, while the estimated values based purely on experimental data are -49.0⁵ and -11.2 kcal/mol,⁴ respectively.

The full reaction profile was then constructed by performing optimizations at the RHF/6-31+G** level at various values of *R*, as described in the Methods. Calculations at MP4/6-311++G**//RHF/6-311++G** were also done for several *R* values, from which a full energy profile was interpolated via a cubic-spline fit. The reason for using this procedure was based on that fact that the reaction profile at lower levels of theory gave a smooth reaction profile that could be easily and accurately fit via a cubic-spline fitting procedure. Furthermore, using this

(22) Weiner, S. J.; Singh, U. C.; Kollman, P. A.; *J. Am. Chem. Soc.* **1985**, *107*, 2219.

(23) (a) Chandrasekhar, J.; Smith, S. F.; Jorgensen, W. L. *J. Am. Chem. Soc.* **1984**, *106*, 6867; **1985**, *107*, 154. (b) Chandrasekhar, J.; Jorgensen, W. L. *J. Am. Chem. Soc.* **1985**, *107*, 2974. (c) Jorgensen, W. L.; Buckner, J. K. *J. Phys. Chem.* **1986**, *90*, 4651. (d) Madura, J. D.; Jorgensen, W. L. *J. Am. Chem. Soc.* **1986**, *108*, 2517. (e) Blake, J. F.; Jorgensen, W. L. *J. Am. Chem. Soc.* **1991**, *113*, 7430.

(24) Gao, J. *J. Am. Chem. Soc.* **1991**, *113*, 796.

(25) Herzberg, G. *Molecular Spectra and Molecular Structure: I. Spectra of Diatomic Molecules*; Van Nostrand: New York, 1939.

(26) Herzberg, G. *Molecular Spectra and Molecular Structure: II. Infrared and Raman Spectra of Polyatomic Molecules*; Van Nostrand: New York, 1945.

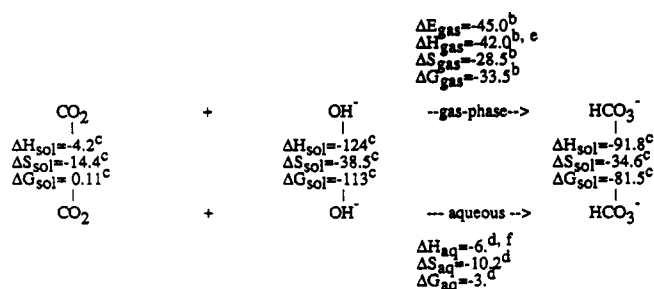


Figure 2. Full thermodynamic cycle at 298.15 K in the gas and aqueous phases. (a) Enthalpy (H) and free energy (G) are in kcal/mol, and entropy (S) is in cal/(mol K). (b) Results are calculated at the RHF/6-311++G**//RHF/6-311++G** level. (c) Experimental data is from ref 20. (d) The predicted thermodynamics changes in the aqueous phase are based on the calculated values in the gas phase at the RHF/6-311++G**//RHF/6-311++G** level and the experimental values of solvation. (e) The estimated experimental heat of formation in the gas phase by Liang and Lipscomb is -49 kcal/mol.⁵ (f) The estimated experimental heat of formation in the aqueous phase by Jönsson *et al.* is -11.2 kcal/mol.⁴

Table IV. Total Energy Profiles

$R/\text{\AA}$	RHF/6-31++G**// RHF/6-31++G** ^a	RHF/6-311++G**// RHF/6-311++G** ^c	MP4/6-311++G**// RHF/6-311++G** ^c
1.4 ^d	-55.1	-51.0	-45.0
1.5	-52.2	-48.4	-46.1
1.6	-46.4	-43.2	-43.6
1.7	-39.9	-36.7	-39.0
1.8	-33.6	-30.8	-34.6
1.9	-28.3	-25.9	-30.8
2.0	-24.1	-22.2	-27.3
2.1	-21.1	-19.5	-24.2
2.2	-18.9	-17.6	-21.5
2.3	-17.2	-16.3	-19.1
2.4	-16.0	-15.2	-17.2
2.7	-13.0	-12.5	-13.3
2.9	-11.2	-11.0	-11.7
3.2	-8.9	-8.8	-9.5
3.4	-7.6	-7.6	-8.1
3.7	-6.0	-6.0	-6.4
3.9	-5.1	-5.0	-5.3
4.4	-3.5	-3.4	-3.6
4.9	-2.5	-2.4	-2.5
5.4	-1.8	-1.8	-2.0
5.9	-1.4	-1.4	-1.6
6.4	-1.0	-1.0	-1.2
6.9	-0.8	-0.7	-0.9
7.4	-0.6	-0.5	-0.7
7.9	-0.5	-0.3	-0.5
8.4	-0.4	-0.2	-0.3
8.9	-0.3	-0.1	-0.2
9.4	-0.3	-0.1	-0.1
9.9	-0.2	0.0	0.0
OH ⁻ + CO ₂	0.0	0.0	0.0

^a In kcal/mol with an absolute energy of OH⁻ + CO₂ of $-263.022\,743\,0$ hartrees. ^b In kcal/mol with an absolute energy of OH⁻ + CO₂ of $-263.097\,299\,0$ hartrees. Values in boldface were calculated, from which the rest were interpolated via a cubic-spline fitting method. ^c In kcal/mol with an absolute energy of OH⁻ + CO₂ of $-263.875\,649\,0$ hartrees. Values in boldface were calculated, from which the rest were interpolated via a cubic-spline fitting method. ^d At the optimized HCO₃⁻ structures at the corresponding basis set.

procedure at the computationally intensive MP4/6-311++G**//RHF/6-311++G** level saved significant amounts of computer time. The calculated energies at several *ab initio* levels are listed in Table IV. The shapes of all of energy profiles are very similar; however, the depths of the profiles decrease as the quality of the *ab initio* treatment increases.

The calculated vibrational frequencies along the RHF/6-31+G** reaction profile are listed in Table V (see Figure 3 also). The first five frequencies (ν_1 – ν_5) at large R values correspond

Table V. Vibration Frequencies (cm⁻¹) along the Reaction Coordinate R at the RHF/6-31+G** Level

$R/\text{\AA}$	ν_1	ν_2	ν_3	ν_4	ν_5	ν_6	ν_7	ν_8
1.4 ^a								
1.5	4189	1963	1348	1270	916.8	742.2	581.8	529.5
1.6	4186	2014	1352	1198	894.7	731.3	537.7	481.0
1.7	4181	2069	1358	1113	871.2	716.7	493.0	439.2
1.8	4174	2129	1367	1018	849.3	697.6	449.3	403.1
1.9	4164	2194	1380	917.9	829.2	675.2	406.6	370.7
2.0	4151	2261	1397	816.5	812.1	648.0	365.1	340.1
2.1	4139	2332	1416	801.5	716.1	629.8	326.4	321.6
2.2	4127	2379	1435	792.0	623.7	611.9	300.8	289.6
2.3	4117	2425	1452	785.0	599.1	542.7	281.6	256.3
2.4	4108	2483	1457	779.7	591.0	474.8	262.3	227.0
2.7	4096	2518	1489	770.7	580.0	340.7	211.5	164.1
2.9	4094	2534	1498	767.3	577.8	287.8	183.8	136.8
3.2	4084	2547	1499	762.9	580.4	232.4	146.4	107.5
3.4	4077	2552	1506	761.4	571.7	205.0	126.0	95.71
3.7	4079	2556	1507	758.9	577.9	174.4	106.4	81.71
3.9	4077	2558	1508	757.7	577.8	156.1	94.65	74.19
4.4	4076	2560	1509	755.4	576.9	116.7	71.40	59.60
4.9	4075	2562	1510	753.8	576.2	88.30	54.94	49.77
5.4	4075	2563	1509	752.7	574.2	71.45	44.11	42.68
5.9	4073	2563	1510	751.9	575.0	60.28	37.73	34.27
6.4	4071	2563	1511	751.4	574.4	52.48	33.76	27.95
6.9	4068	2563	1511	751.2	573.5	44.90	30.26	23.08
7.4	4064	2564	1511	750.7	572.8	36.99	27.00	19.40
7.9	4058	2564	1511	750.5	572.0	29.86	23.56	16.67
8.4	4052	2564	1511	750.3	571.2	25.09	19.26	14.06
8.9	4045	2564	1511	750.2	570.5	22.32	14.87	12.16
9.4	4040	2564	1511	750.1	569.8	20.33	11.26	10.58
9.9	4034	2564	1511	750.0	569.4	18.71	9.284	8.395
	4075 ^b	2905 ^c	1517 ^c	805.4 ^c	805.4 ^c			

^a At the optimized HCO₃⁻ geometry, the calculated full vibrational modes are 4195, 1910, 1465, 1337, 1023, 932.1, 711.6, 623.5, and 587.0 cm⁻¹, respectively. ^b The calculated OH⁻ frequency. ^c The calculated CO₂ frequencies.

to the calculated frequencies of isolated OH⁻ and CO₂ qualitatively, but not quantitatively (4034, 2564, 1551, 750.0, and 569.4 cm⁻¹ vs 4075, 2905, 1517, 805.4, and 805.4 cm⁻¹). Conceptually, we might expect better agreement; however, the observed differences can be explained in the following way. When R is large, the energy gradient vector becomes very small so that its direction is less well defined, and the projection operator \mathbf{P} is, therefore, not accurately determined. This leads to errors in the frequency calculation. When R is close (say, $R = 1.5$ Å) to the value of the optimized structure, the calculated frequencies approach the full normal modes calculated at the optimized structure, but with one less mode. In this case the energy gradient vector is quite large, so the projection operator \mathbf{P} is well defined in this case. The correspondence of our reaction coordinate R with a normal mode of HCO₃⁻ is not exactly true unless the direction of the energy gradient vector is parallel with the direction of one of the normal modes of the optimized structure (this is unlikely since R is definitely not a normal mode coordinate for the fully minimized HCO₃⁻). It is also important to notice that three modes (ν_6 – ν_8) which are related to the relative motion between OH⁻ and CO₂ approach zero when R becomes large. This makes the harmonic oscillator approximation^{7,8} used in the thermodynamic calculation invalid after $R = 2.4$ Å because at least one vibration mode drops below kT (which is about 200 cm⁻¹ at 298 K). Fortunately all interesting features for this reaction occur before $R = 2.4$ Å and the conclusions from our study do not suffer from this breakdown of the harmonic oscillator assumption at large R . The enthalpy (H) and the entropy contribution (TS) from the molecular translations, rotations, and vibrations are listed in Table VI and plotted in Figure 3. The H profile has a discontinuity at $R = 1.4$ Å which is caused by the fact that the minimized structure has one more vibration mode. Since H is mostly dominated by the zero-point energy of high-frequency vibrational modes, it is not surprising to see that H at large R approaches the value of the isolated OH⁻ and CO₂.

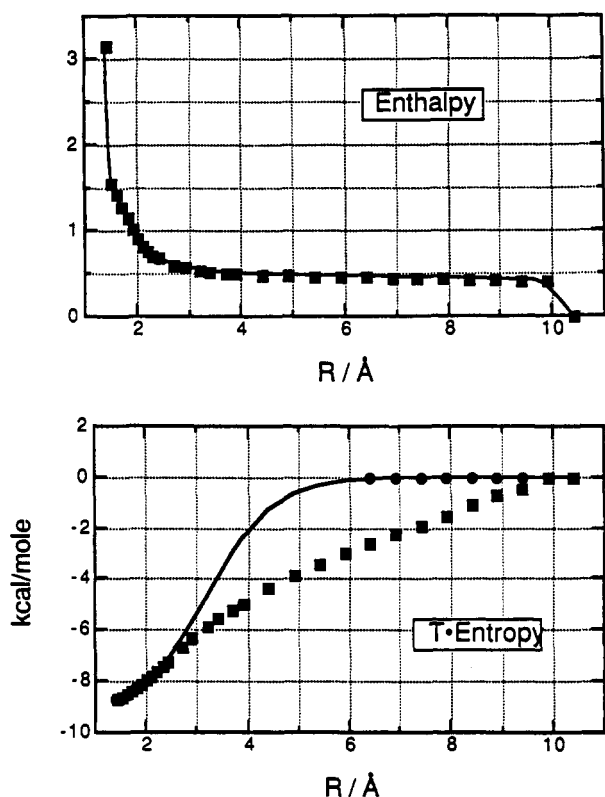


Figure 3. (top) Calculated enthalpy contribution from the molecular vibrational frequencies at 298.15 K. The last point at $R = 10.4$ Å indicates isolated $\text{OH}^- + \text{CO}_2$. Both end points ($R = 1.5$ and 9.9 Å) show discontinuities (see text). (bottom) Calculated entropy contribution from the molecular vibration frequencies at 298.15 K. Squares indicate the calculated values. Circles indicate the expected asymptotic values after $R = 6.4$ Å. The line is fitted from the calculated points between 1.4 and 2.4 Å and the asymptotic points after 6.4 Å. See the text for further discussion.

Since the shape of the H curve is quite reasonable, it is directly used without any modification in the construction of the free energy profile in the gas phase.

For the entropy (S), we have the opposite situation. When the vibration frequencies are larger than kT , their entropy contributions are very small. This explains why there is hardly any evidence of a discontinuity in TS at $R = 1.4$ Å (see Figure 3b). However, when the vibrational frequencies are less than kT , their entropy contributions become quite large and eventually diverge when $h\nu/kT$ goes to zero.²⁷ We can also see that the shape of the calculated TS curve becomes almost linear with R , which is nonphysical. In order to obtain a better TS profile, we have assumed that after $R = 6.4$ Å the $\text{OH}^-\cdots\text{CO}_2$ complex is essentially composed of isolated OH^- and CO_2 molecules, which, therefore, have the same entropy as that of isolated OH^- and CO_2 . Then we use a function to smoothly connect the TS values from 1.4 to 2.4 Å and from 6.4 to 9.9 Å (see Table VI and Figure 3 for details of the fit). The newly obtained TS profile is then used in the construction of the free energy profile in the gas phase.

In Figure 4, the profiles of the gas-phase total energy at the MP4/6-311++G**//RHF/6-311++G** level and also the enthalpy (H) and entropy contributions (TS) are given. The free energy profile (G_{gas}) for this reaction is then constructed as $G_{\text{gas}} = E + H - TS$. In the gas phase there is no free energy barrier on going from isolated OH^- and CO_2 to the optimized HCO_3^- , which confirms the results from previous studies.^{4,5}

3.2. Aqueous-Phase Profile. In order to estimate the solvent-induced free energy barrier, we have carried out MD-FEP simulations.¹⁰⁻¹¹ In the present study, the solvation free energy

Table VI. Thermodynamic Corrections (at 298.15 K) along the Reaction Coordinated at the RHF/6-31+G** Level

$R/\text{\AA}$	H^a	TS^b	$TS(\text{fit})^c$
1.4 ^d	3.0	-8.5	-8.5
1.5	1.6	-8.4	-8.4
1.6	1.4	-8.3	-8.3
1.7	1.3	-8.2	-8.2
1.8	1.1	-8.1	-8.1
1.9	1.0	-7.9	-7.9
2.0	0.9	-7.8	-7.8
2.1	0.8	-7.6	-7.6
2.2	0.8	-7.4	-7.4
2.3	0.7	-7.2	-7.2
2.4	0.7	-7.0	-7.0
2.7	0.6	-6.5	-6.2
2.9	0.6	-6.1	-5.6
3.2	0.5	-5.7	-4.6
3.4	0.5	-5.4	-3.9
3.7	0.5	-5.0	-2.9
3.9	0.5	-4.8	-2.4
4.4	0.5	-4.2	-1.3
4.9	0.5	-3.6	-0.6
5.4	0.5	-3.2	-0.3
5.9	0.5	-2.8	-0.1
6.4	0.5	-2.4	0.0
6.9	0.5	-2.0	0.0
7.4	0.4	-1.7	0.0
7.9	0.4	-1.3	0.0
8.4	0.4	-0.9	0.0
8.9	0.4	-0.5	0.0
9.4	0.4	-0.2	0.0
9.9	0.4	-0.0	0.0
$\text{OH}^- + \text{CO}_2$	0.0	0.0	0.0

^a Enthalpy (H) with a reference value at $\text{OH}^- + \text{CO}_2$ of 15.5 kcal/mol. ^b Entropy contribution (TS) with a reference value at $\text{OH}^- + \text{CO}_2$ of 27.5 kcal/mol. ^c Fitted TS . Values in boldface were used in the fitting to the function $TS = a + \{b/[1 + \exp[-\beta(R-d)]]\}$, where $a = 0.01$ kcal/mol, $b = -9.22$ kcal/mol, $\beta = 1.533 \text{ \AA}^{-1}$, and $d = 3.22 \text{ \AA}$. ^d At the optimized HCO_3^- geometry with the full $3N - 6$ set of vibrational modes.

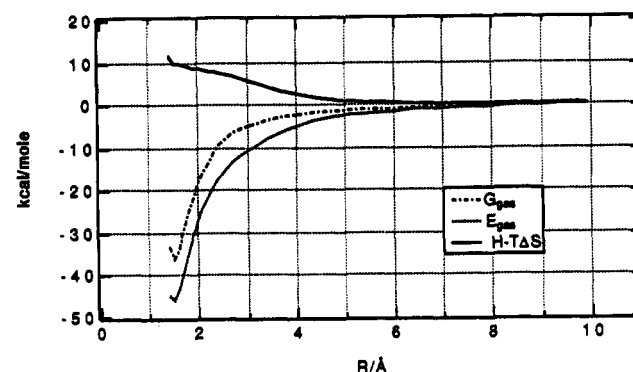


Figure 4. Gas-phase thermodynamic profiles at 298.15 K. E_{gas} is the total energy, $H - T\Delta S$ is the thermodynamic correction to the total gas-phase energy, and G_{gas} is the gas-phase free energy profile.

is approximated by the free energy change between the following two thermodynamic states: (A) a box of water with a rigid $\text{OH}^-\cdots\text{CO}_2$ complex outside the box and (B) a box of water with the same complex inside. In other words, we are calculating the absolute free energy of solvation for these complexes. Determining the absolute free energies of solvation in this way as opposed to calculating the relative solvation free energies between two adjacent points may introduce more noise in the calculations. However, we have used rather long simulations (180 ps) to determine our absolute free energies of solvation and have found that the hysteresis in these calculations is small relative to the value obtained in most cases (see Table VIII). This suggests that the noise in our calculations will only have a modest effect on our calculated results. The effect of water molecules on the properties (geometry, charge distribution, and molecular vibrational, ro-

(27) McQuarrie, D. *Statistical Mechanics*; Harper & Row: New York, 1976.

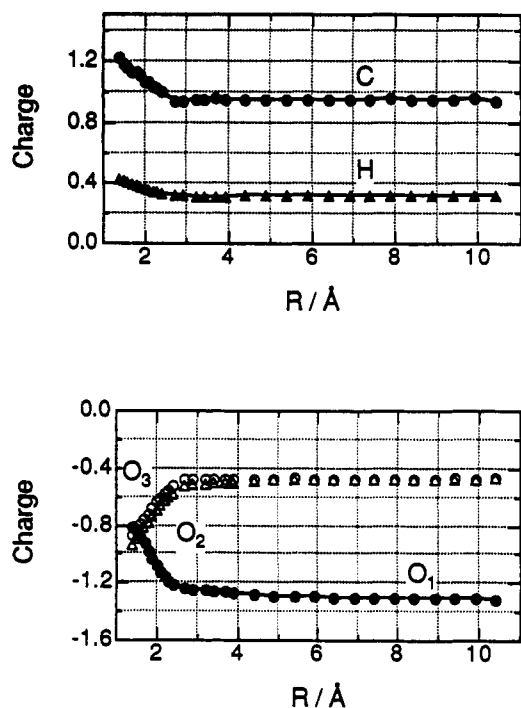


Figure 5. Variation of ESP-derived atomic point charges obtained at the RHF/6-31+G** level along the reaction coordinate R .

tational, and translational motion) of the solute complex is not considered in this study, and we use the geometry and charge distribution obtained in the *ab initio* gas-phase calculations.

The solvent molecules interact with the solute $\text{OH}^- \cdots \text{CO}_2$ complex via van der Waals and electrostatic interactions, and it is clear that the strength of these interactions will vary along the reaction profile. Hence, the nonbond parameters are expected to vary accordingly along the reaction coordinate R . The ESP-derived atomic point charges¹⁴ at the *ab initio* RHF/6-31+G** level were used to account for the variation in the charge distribution along the reaction coordinate (Figure 5). However, we have no knowledge of the van der Waals parameters between the water molecules and the solute $\text{OH}^- \cdots \text{CO}_2$ complex at every point along the reaction profile. Since the solvation free energies of HCO_3^- , OH^- , and CO_2 have been measured experimentally,²⁰ we have used them to calibrate the van der Waals parameters for the end points (HCO_3^- , OH^- , and CO_2). We have not determined the absolute solvation free energies of these species in conjunction with a correction for long-range electrostatics (e.g. Born correction, Ewald sums, etc.) but have rather determined parameters that give the correct absolute solvation free energy given a cutoff distance of 8 Å. This was done because it is difficult to apply the Born correction for the intermediate points along the reaction coordinate and it is more expensive to use Ewald sums in the FEP simulations. Moreover, we are interested in relative numbers and it is our expectation that we would obtain similar numbers regardless of which method was employed. In Table VII, the end point van der Waals parameters are listed along with the corresponding solvation free energy changes calculated using these parameters. Next we assumed that the variation of the van der Waals parameters of the $\text{OH}^- \cdots \text{CO}_2$ complex along the reaction profile has an exponential functional form $p_0 + (p_1 - p_0)[1 - \exp\{-\beta(R - R_0)\}]$ (p_0 and p_1 are the two end point values of the van der Waals parameter, $\beta = 0.9512 \text{ Å}^{-1}$, and $R_0 = 1.3949 \text{ Å}$). From this expression the parameter values in between the end points were interpolated readily (see Figure 6). After observing that the *ab initio* energy and also the ESP charges had similar functional forms, we decided that this is a reasonable approximation for the behavior of the van der Waals parameters. Furthermore, Madura and Jorgensen have used data from *ab initio* calculations to determine interaction energies between a

Table VII. Nonbond Parameters for OH^- , CO_2 , and HCO_3^-

	OH^-	CO_2	HCO_3^-
charges ^a	0.3167 H—O -1.3167	-4656 O=C=O 0.9312	H 0.4194 O ₁ -0.8192 C 1.2149 O ₂ -0.9424 O ₃ -0.8727
vdW parameters ^b	1.0/0.0 H—O 1.64/1.52	1.4/18 O=C=O 1.9/13	H 1.0/0.0 O ₁ 1.5246/152 C 1.4805/2558 O ₂ 1.8719/1171 O ₃ 1.4805/2558
calcd ΔG_{sol}^c	-112.9 (0.3)	0.31 (0.5)	-83.8 (0.5)
exptl ΔG_{sol}^d	-113	0.11	-81.5

^a ESP-derived atomic point charges obtained at the RHF/6-31+G**//RHF/6-31+G** level. ^b R values are in Å, and e values are in kcal/mol. ^c Solvation free energy in kcal/mol. The values in parentheses are the differences between the forward and backward MD-FEP simulations. ^d See ref 20.

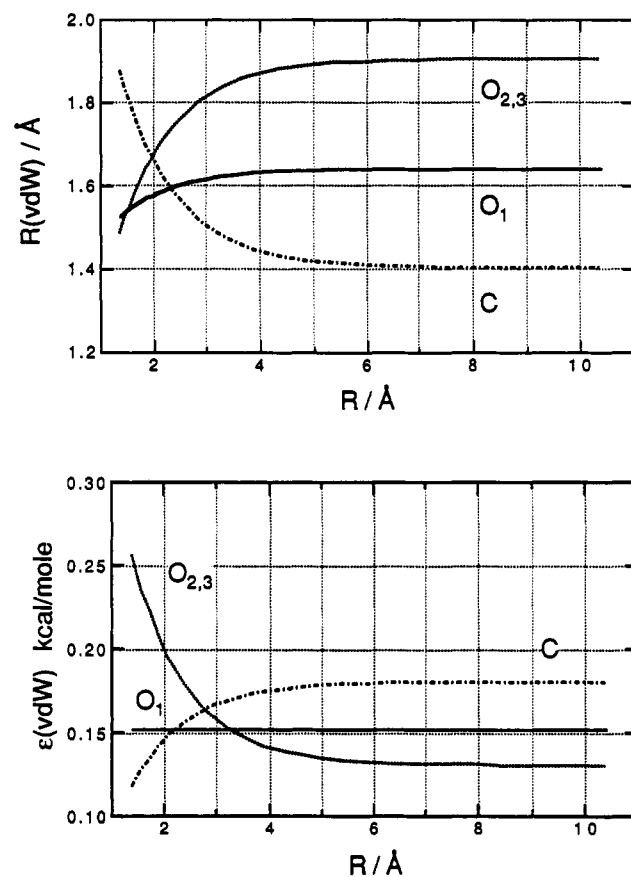


Figure 6. The variation of the van der Waals parameters along the reaction coordinate R . $R(\text{vdW})$ is the van der Waals radius, and $\epsilon(\text{vdW})$ is the well depth.

solute molecule and a single water molecule to derive the charges and van der Waals parameters for the solute-solvent interactions along the reaction path of the solute complex.^{23d} It is reassuring to note that their nonbond parameters have a similar behavior along the reaction coordinate as do ours.

The calculated solvation free energies along the reaction coordinate are given in Table VIII. For large R , we initially expected the calculated solvation free energy to approach the value obtained at the end point $\text{OH}^- + \text{CO}_2$ (-113 kcal/mol). It turned out that at $R = 6.4$ and 9.9 Å the calculated values were lower (-118 and -121 kcal/mol, respectively) than the experimental value. We went back to the nonbond cutoff scheme used in our MD-FEP calculations and discovered that it was responsible for this discrepancy. According to the cutoff scheme used, water molecules within an 8-Å radius of the solute $\text{OH}^- \cdots \text{CO}_2$ complex

Table VIII. Calculated Free Energy Profiles along the Reaction Coordinate R

$R/\text{\AA}$	ΔG_{sol}^a	ΔG_{gas}	$G_{\text{aq}} = \Delta G_{\text{gas}} + \Delta G_{\text{sol}}$
1.4	28.8 (0.5)	-33.5	-4.7
1.5	33.6 (0.4)	-36.1	-2.5
1.6	38.7 (0.5)	-33.9	4.8
1.7	40.9 (0.1)	-29.5	11.4
1.8	41.2 (0.7)	-25.4	15.8
1.9	39.1 (0.7)	-21.9	17.2
2.0	37.8 (0.8)	-18.6	19.2
2.1	33.3 (1.1)	-15.8	17.5
2.2	30.0 (0.5)	-13.3	16.7
2.4	22.7 (0.4)	-9.5	13.1
2.7	17.3 (0.8)	-6.5	10.8
2.9	13.1 (1.4)	-5.5	7.6
3.4	7.9 (0.9)	-3.7	4.2
3.9	4.4 (1.9)	-2.4	2.0
4.4	1.2 (2.1)	-1.8	-0.6
6.4	0.0	0.0	0.0
9.9	0.0	0.0	0.0
$\text{OH}^- + \text{CO}_2$	-112.6(0.8)	0.0	0.0

^a Calculated solvation free energy in kcal/mol with respect to $\text{OH}^- + \text{CO}_2$, which has a reference value of -112.6(0.8) kcal/mol. The numbers in parentheses are the hystereses between the forward and backward MD-FEP simulations.

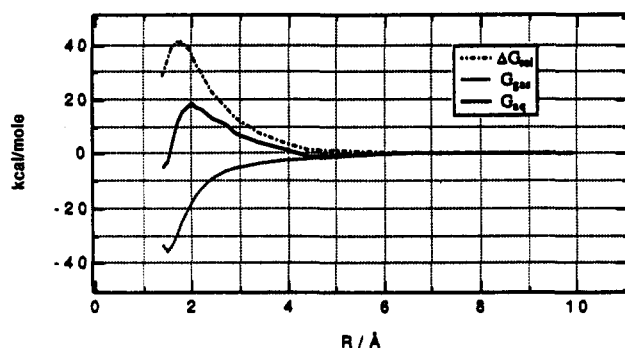


Figure 7. The free energy profiles for the $\text{OH}^- + \text{CO}_2 \rightarrow \text{HCO}_3^-$ reaction at 298.15 K. G_{gas} is the gas-phase free energy, ΔG_{sol} is the solvation free energy, and G_{aq} is the total free energy in the aqueous phase. $\text{CO}_2 + \text{OH}^-$ has been chosen as the zero point.

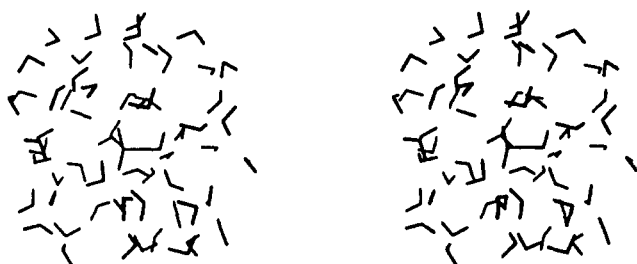


Figure 8. A snapshot of the solvent structure around the point where $R = 2.0 \text{ \AA}$.

would interact with the solute complex, while at $R = 9.9 \text{ \AA}$, we have isolated OH^- and CO_2 . OH^- should interact only with solvent molecules within the 8- \AA sphere centered on OH^- , and CO_2 should interact only with solvent molecules within the 8- \AA sphere centered on CO_2 . However, the cutoff scheme we used also allowed OH^- to interact with solvent molecules within the sphere centered on CO_2 , and *vice versa*. This is due to the fact that we had a fictitious bond between the CO_2 and OH^- which gave the appearance of having only one solute molecule even at long distances. In order to finally confirm that the extra nonbonded interactions were responsible for the observed discrepancy, we conducted new MD-FEP runs, with OH^- and CO_2 as two individual solute molecules fixed relative to one another (the O of OH^- and the C of CO_2 were the only atoms restrained). In this way, no extra nonbond interaction would be included. The new results obtained for R

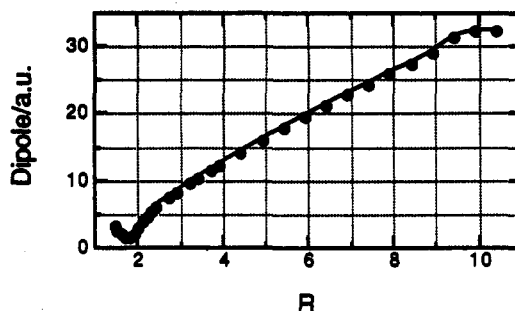


Figure 9. The electric dipole moment obtained at the RHF/6-31+G** level as a function of the reaction coordinate. The minimum is located at $R = 1.8 \text{ \AA}$.

= 6.4 and 9.9 \AA were -112 and -114 kcal/mol, respectively. Hence, this resolved the observed discrepancy in our MD-FEP simulations.

The relative solvation free energy profile is given in Table VIII with the zero point chosen at $\text{OH}^- + \text{CO}_2$. On the basis of the results described above, the relative values at $R = 6.4$ and 9.9 \AA were set to zero. Finally, we combined the gas-phase and solution-phase free energy profiles to construct the total free energy profile (see Table VIII and Figure 7). The maximum point of the relative solvation free energy profile is located at $R = 1.8 \text{ \AA}$, with a value of 41 kcal/mol with respect to the $\text{OH}^- + \text{CO}_2$ end point. This indicates that some of the water molecules hydrating OH^- have to be stripped off in order to react with CO_2 and that the penalty for doing this is on the order of 41 kcal/mol. Inspection of radial distribution (rdf) profiles obtained from MD simulations at the two end points and at 2.0 \AA (the TS for the total free energy profile) shows that as we go from $\text{CO}_2 + \text{OH}^-$ the hydroxyl group loses interactions with the surrounding water molecules as we reach the transition state (TS). At the TS and the 9.9- \AA point, the CO_2 oxygens do not show any indications of strong interactions with the surrounding water molecules. Hence, we conclude that the loss of water molecules hydrating the hydroxyl group, to a large extent, gives rise to the solvent-induced barrier. Once we pass through the TS and proceed onto the bicarbonate ion we find that the solvent structure around the "CO₂ oxygens" becomes quite substantial, as it is for the hydroxyl fragment. A snapshot of the water structure around the TS structure is given in Figure 8.

The observed solvation free energy profile mimics the behavior of the electric dipole moment, which is observed to have a minimum at $R = 1.8 \text{ \AA}$, where the solvation profile has a maximum (see Figure 9). Hence, the solvation free energy is, not unexpectedly, related to the variation of the charge distribution along the reaction profile. The maximum point on the total free energy profile is located at $R = 2.0 \text{ \AA}$ with a value of 19.2 kcal/mol with respect to the $\text{OH}^- + \text{CO}_2$ end point. Interestingly, the position of the solution-phase transition state is similar to that observed by others for the reactions of OH^- with formaldehyde and formamide.^{22,23d} The calculated barrier height is ~7 kcal/mol larger than the experimental value of 12.1 kcal/mol.²⁸ The ΔG_{rxn} is computed to be ~5.0 kcal/mol, while experimentally it is ~-9 kcal/mol (see Figure 2). There are many possible sources which might be able to account for the difference between our calculated and experimental barrier heights, but the most significant is likely to be the neglect of polarization effects in this charged system.^{29,30} It is interesting to note that Miertus and co-workers calculated

(28) (a) Amdur, I.; Hamnes, G. G. *Chemical Kinetics, Principles and Selected Topics*; McGraw-Hill: New York, 1966; pp 48-58. (b) Boudart, M. *Kinetics of Chemical Process*; Prentice-Hall: Englewood Cliffs, NJ, 1968; pp 35-46. (c) Kreevey, M. M.; Truhlar, D. G. In *Investigation of Rates and Mechanisms of Reactions*; Bernasconi, C. F., Ed.; Techniques of Chemistry, 4th ed., Vol. VI, Part 1; Wiley-Interscience: New York, 1986. (d) We used the methods from (a)-(c) and redid the fit to the data in ref 2. At the location of the transition state (TS), the thermodynamic potentials with respect to the isolated $\text{OH}^- + \text{CO}_2$ configuration are $\Delta H_{\text{TS}} = 12.6 \text{ kcal/mol}$, $\Delta S_{\text{TS}} = 1.75 \text{ cal/(mol K)}$, and $\Delta G_{\text{TS}} = 12.1 \text{ kcal/mol}$.

the energy barrier height to be over twice as large (26.6 kcal/mol) as the experimental value using a continuum model,⁶ while Aqvist *et al.*, using the EVB approach, have recently obtained a reasonable representation of this reaction in solution.³¹

4. Summary

In this work, we performed *ab initio* calculations on the $\text{OH}^- + \text{CO}_2$ gas-phase reaction using large *ab initio* basis sets. The finite temperature contributions from the molecular vibrations, rotations, and translations were found to be quite significant. The calculated gas-phase free energy profile shows no barrier, which confirms the finding of previous workers that this reaction is activationless in the gas phase. By combining experimental values for the thermodynamic changes of solvation and calculated values for thermodynamic changes in the gas phase, we were able to construct the full thermodynamic cycle for this reaction (Figure 2). The thermodynamic changes of reaction in the aqueous phase are then predicted to be $\Delta H_{\text{aq}} = -6$ kcal/mol (-11.2 kcal/mol has been estimated from experiment information⁴), $\Delta S_{\text{aq}} = -10.2$ cal/(mol K), and $\Delta G_{\text{aq}} = -3$ kcal/mol.

Using MD-FEP simulations we have assembled a free energy of solvation profile which gives a maximum of ~ 40 kcal/mol at ~ 1.8 Å. From consideration of the solvent structure around the end points and at the solvation free energy profile *TS*, we conclude that the loss of solvation around the incoming hydroxide ion results in the substantial solvation free energy barrier. Moreover, it does not appear that the generation of negative charge on the CO_2 oxygens can compensate for the loss of solvent interaction with the hydroxide ion. Using the gas-phase free energy profile

in conjunction with the solvation free energy profile allows us to generate the free energy profile for this reaction in aqueous solution. The resulting profile gives a barrier of 19.2 kcal/mol, which is in fair agreement with the experimental value of 12.1 kcal/mol. The ΔG_{rxn} is calculated to be ~ -5 kcal/mol, while the experimental value is closer to -9 kcal/mol.

From this study and our other theoretical investigations of HCAII, we are beginning to be able to gain molecular-level insights into the catalytic efficiency of this enzyme.³²⁻³⁵ The $\text{CO}_2 + \text{OH}^-$ reaction has a very low barrier in solution (~ 12.1 kcal/mol), and the enzyme reduces this barrier height by about a factor of 2.³⁶ From the present study we have found that the reaction of hydroxide with CO_2 is activationless in the gas phase. This strongly suggests that there are no electronic reasons why this reaction should not occur readily. In an aqueous environment, on the other hand, we have found that as OH^- approaches CO_2 water molecules are displaced from the hydroxide ion, which results in a substantial free energy barrier. This suggests that desolvation effects are the main reason why there is a barrier to this reaction in solution.^{4,5,9} Hence, for the enzyme to carry out its function efficiently, it should provide an hydroxide ion in an environment where desolvation will not play a dominating role. HCAII accomplishes this by using a zinc ion and suitably placed active site residues (*i.e.* Thr 199) to stabilize the hydroxide ion in a relatively hydrophobic pocket. Hence, the desolvation of the hydroxide ion does not play as important of a role in the enzyme as it does in free solution. Other factors are important (*e.g.* substrate orientation, entropic factors, *etc.*) for efficient catalysis by HCAII, but desolvation appears to be a key difference between the enzymatic and solution-phase reactions.^{4,5,9}

Acknowledgment. We thank the NIH for supporting this work (GM44974) and the Pittsburgh Supercomputer Center for generous allocations of CRAY Y-MP computer time. Helpful discussions with Przemyslaw Maslak, Dr. Y. J. Zheng, and Dr. K. V. Damodaran are also acknowledged.

(29) (a) Caillol, J. M.; Levesque, D.; Weis, J. J.; Kusalik, P. G.; Patey, G. N. *Mol. Phys.* **1985**, *55*, 65; **1987**, *62*, 1225. (b) Howard, A. E.; Singh, U. C.; Billeter, M.; Kollman, P. A. *J. Am. Chem. Soc.* **1988**, *110*, 6984. (c) Angyan, J. G.; Colonna-Cesari, F.; Tapia, O. *Chem. Phys. Lett.* **1990**, *116*, 180. (d) Straatsman, T. P.; McCammon, J. A. *Mol. Simul.* **1990**, *5*, 181; *Chem. Phys. Lett.* **1990**, *167*, 252; *177*, 433. (e) Sprik, M.; Klein, M. L. *J. Chem. Phys.* **1988**, *89*, 7556. Sprik, M. *J. Phys. Chem.* **1991**, *95*, 2283. Watanabe, K.; Klein, M. L. *Chem. Phys.* **1989**, *131*, 157.

(30) (a) Car, R.; Parrinello, M. *Phys. Rev. Lett.* **1985**, *55*, 2471. (a) Singh, U. C.; Kollman, P. *Proc. Natl. Acad. Sci. U.S.A.* **1986**, *83*, 6402. (a) Singh, U. C.; Kollman, P. *J. Comput. Chem.* **1986**, *7*, 718. (b) Bash, P.; Field, M.; Karplus, M. *J. Am. Chem. Soc.* **1987**, *109*, 8092. (c) Field, M.; Bash, P.; Karplus, M. *J. Comput. Chem.* **1990**, *11*, 700.

(31) Aqvist, J.; Fothergill, M.; Warshel, A. *J. Am. Chem. Soc.* **1993**, *115*, 631.

(32) Merz, K. M., Jr. *J. Am. Chem. Soc.* **1990**, *112*, 7973.

(33) Merz, K. M., Jr.; Hoffmann, R.; Dewar, M. J. S. *J. Am. Chem. Soc.* **1989**, *111*, 5636.

(34) Merz, K.M., Jr. *J. Mol. Biol.* **1990**, *214*, 799.

(35) Zheng, Y. J.; Merz, K. M., Jr. *J. Am. Chem. Soc.* **1992**, *114*, 10498.

(36) Behravan, G.; Jonsson, B.-H.; Lindskog, S. *Eur. J. Biochem.* **1990**, *190*, 351.